

Article

Volatilization Behavior of Manganese from Molten Steel with Different Alloying Methods in Vacuum

Jianhua Chu and Yanping Bao *

State Key Lab of Advanced Metallurgy, University of Science & Technology Beijing, No.30 Xueyuan Road, Haidian District, Beijing 100083, China; B20180527@xs.ustb.edu.cn

* Correspondence: 18811389812@163.com; Tel.: +86-138-1076-8855

Received: 31 August 2020; Accepted: 2 October 2020; Published: 9 October 2020



Abstract: The volatilization loss of manganese during the vacuum smelting process is one of the key factors that determines the manufacturing cost and quality of manganese steel. In this study, the laboratory experiments and thermodynamic calculations were performed to investigate volatilization behavior of manganese from molten steels with different alloying methods in vacuum process. Based on the thermodynamic analysis, with the increase of manganese content, the partial vapor pressure of the manganese component increased, resulting in manganese being easily volatilized from molten steel. The carbon content in the steel shows an evident influence on partial vapor pressure of manganese component, and a higher carbon content in steel leads to a lower partial vapor pressure of manganese, but it not influenced by the silicon content. Compared with the alloying method of high carbon ferromanganese, the volatilization loss of manganese in the alloying method of silicon manganese presents faster decay, agreeing well with the thermodynamic analysis. Besides, the volatile fraction generated in the alloying method of high-carbon ferromanganese is composed of a large amount of MnO nanorods with a lateral length approximately 500 nm and a small number of Mn₃O₄/Mn nanoparticles with a diameter less than 500 nm. Additionally, the volatile fraction generated in the alloying method of silicon manganese shows Mn₃O₄ nanoparticles as the main phase. It can be inferred that the existence of the manganese oxide phase is attributed to the high chemical activity of nanoscale particles within air.

Keywords: volatilization behavior; manganese; vapor pressure; alloying methods; volatile fraction

1. Introduction

Manganese is an indispensable alloying element in steel, owing to its ability to significantly improve the strength and toughness of steel through solid solution strengthening and dispersion strengthening mechanisms [1,2]. In particular, medium manganese steels (5–12 wt% Mn) as the third-generation advanced high-strength steels (AHSS) are in the limelight, and this is attributed to their exhibiting extraordinary combination of ultra-high strength, excellent plasticity, and low production costs, leading to great applications in automotive, construction, and high-speed trains industries [3–6]. In recent years, the microstructure and mechanical properties of medium manganese steels have been extensively studied [7,8]. However, compared with traditional steels, there are few publications of the smelting process depending on alloying composition like Mn, C, Al, Cr, Mo, Si, N, and V to produce these steel grades. Specifically, the control of high yield and narrow composition of manganese in the smelting process plays an important role in final steel quality and costs of raw materials.

The Ruhrstahl-Heraeus (RH) process was developed for degassing, decarbonization, efficient alloying, inclusion removal, and rapid homogenization of the molten steel, and now it is widely used to achieve high cleanliness for the industrial manufacture of high-quality manganese steels [9,10]. In this

process, the complex reactions among molten steel, gas, inclusions, and refractory make it difficult to precisely control the final steel composition, caused by fluctuations in alloying elements; yields [11,12]. Accordingly, the migration path of manganese element in molten steel during vacuum treatment is divided into four stages, as shown in Figure 1: (i) as alloying element, (ii) oxidation of molten steel to form inclusions, (iii) vacuum evaporation, and (iv) lightweight alloy powder is pumped away by vacuum. Therefore, the volatilization loss of manganese under high temperature and vacuum is one of the key factors to cause unstable manganese yield, which may give some helpful information for the control of steel composition. On the other hand, the interaction behaviors between the volatile fraction contain manganese and the refractories are generally considered harmful to vacuum chamber service life, vacuum pumping capacity, and emissions indicators, which results in great hidden safety hazard to production [13,14]. Besides this, the molten steel inevitably suffers from secondary pollution caused by flaking of volatile fraction from the inner wall of the vacuum chamber, increasing the inclusions and oxygen content in the steel [15], seriously affecting the cleanliness of the steel. Nevertheless, the volatile loss of manganese from molten steel under vacuum treatment has rarely been studied. Hence, it is extremely urgent that attention should be paid to the volatilization behavior of manganese from medium-manganese steel under vacuum.

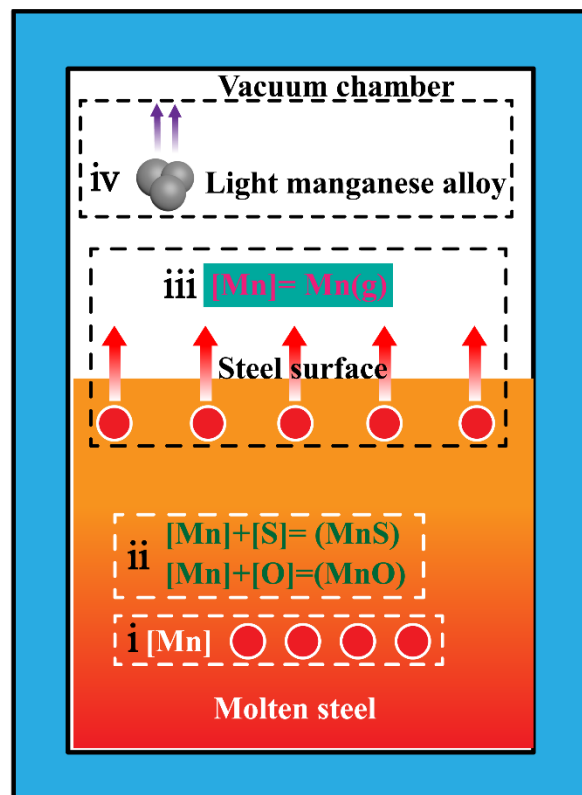


Figure 1. Migration path of manganese element during vacuum treatment of molten manganese steels: (i) as alloying element, (ii) oxidation of molten steel to form inclusions, (iii) vacuum evaporation, and (iv) lightweight alloy powder is pumped away by vacuum.

In the current study, the theoretical saturation vapor pressure of manganese in molten manganese steel was thermodynamically discussed. The effects of different time and alloying elements on the variation of manganese content in molten steel by the addition of different manganese alloys under vacuum were extensively investigated by the lab experiment. Meanwhile, the obtained volatile fraction of manganese was further characterized. This work provides an improved understanding of the volatilization behaviors of manganese and theoretical basis for the stable control of manganese yield during industrial vacuum secondary refining of medium-manganese steels.

2. Experimental Procedure

2.1. Experimental Materials

The typical IF (interstitial free) steel and manganese alloy were supplied by Baogang Group (China) and Ningbo Iron and Steel Co., Ltd. (China), respectively. The corresponding chemical composition is shown in Table 1.

Table 1. Main chemical composition of raw materials (wt%), IF = interstitial free.

Component	(C)	(Si)	(Mn)	(P)	(S)	(Al)
IF steel	0.004	0.005	0.137	0.017	0.009	0.036
High-carbon ferromanganese	≤8.0	≤2.0	75.0	≤0.2	≤0.05	-
Silicon manganese	≤1.8	20.5	77.2	≤0.2	≤0.04	-

2.2. Vacuum Experiment Procedure

The manganese volatilization experiment was conducted on a 10 kg vacuum induction furnace (Figure 2), which consists of a vacuum system, smelting system, sampling/alloying system, pulling system, and cooling system. During experiment, an IF-steel sample was put into a high-purity magnesia crucible (inner diameter, 110 mm; outer diameter, 130 mm; and height, 195 mm), which was assembly positioned crucible-coil in the center of a water-cooled vacuum chamber. The chamber was then vacuumed completely by a mechanical pump, followed by backfill argon to 60 KPa. To ensure there was no residual air in the vacuum chamber, the above process was repeated several times. Subsequently, the IF-steel block was heated by induction heating via adjusting the power. When the temperature reached 1873 K, manganese alloy packed in a tie foil was added into the melt. After homogenization of molten steel for 4 min, the first sample was taken by a cylinder sampler and quenched in water. At this time, the chamber continuously was vacuumed to about 530 Pa. The other two samples were taken at 20 and 40 min, respectively. Two sets of experiments were performed at the same experimental procedure, except for the amount of addition of IF steel and manganese alloy (Table 2). Finally, the manganese steel melt was poured in a mold with the protection of argon. After completion of each experiment for 10 min until the completely solidified, the vacuum furnace was cooled to room temperature, in the air, by opening the furnace door, and the volatile fraction was collected in the vacuum chamber wall.

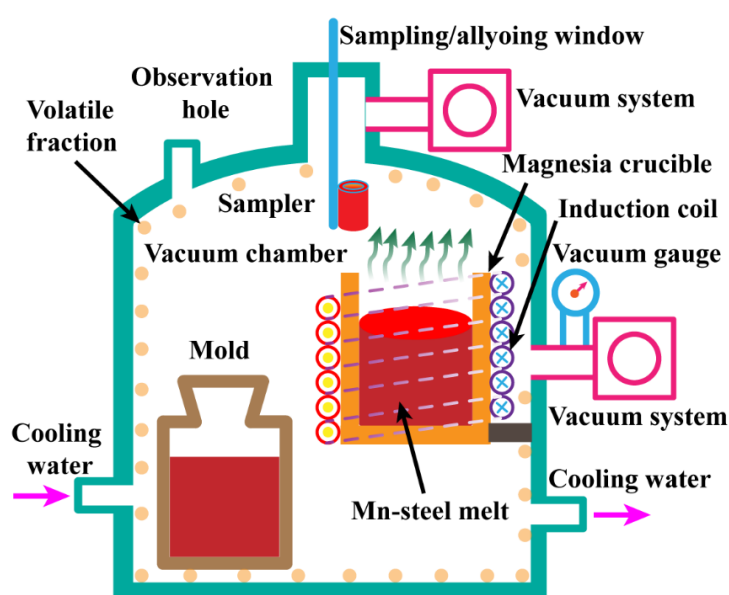


Figure 2. Schematic diagrams of the vacuum induction furnace.

Table 2. Preparation of molten-steel composition with different alloying methods.

No.	IF Steel (kg)	High-Carbon Ferromanganese (kg)	Silicon Manganese (kg)
1	4.5	-	0.781
2	4.54	0.838	-

2.3. Sample Characterization

The chemical compositions of the as-obtained manganese steel ingots and steel samples were evaluated by the inductive coupled plasma (ICP, PerkinElmer Analyst ICP-OES 8300, Waltham, Massachusetts, USA,) and direct reading spectrometer. The manganese element distribution of steel ingots was also characterized by electron probe microstructure analysis (EPMA, JXA-Isp100, Tokyo, Japan). Phase compositions of the volatile fraction were analyzed by powder X-ray diffraction (XRD, Smart-lab, Tokyo, Japan), employing a scan rate of $10^\circ \text{ min}^{-1}$ from 10° to 90° with Cu $K\alpha$ radiation. Meanwhile, morphologies of manganese alloy and volatile fraction were characterized by field-emission scanning electron microscopy (FESEM, Hitachi SU8010, Tokyo, Japan) equipped with X-ray energy-dispersive spectrometry (EDS).

3. Results and Discussion

3.1. Thermodynamic Analysis

The fundamental physical volatilization of metal elements from the steel can occur in a specific temperature range, which is based on the principle that the saturation vapor pressure significantly contributes to the evaporation characteristics. In general, the higher the saturated vapor pressure of the element, the easier it is to volatilize it. According to the Clausius–Clapeyron relation, the saturation vapor pressure of a pure substance can be calculated by Equation (1) [16]:

$$\log p^* = AT^{-1} + B \lg T + CT + D \quad (1)$$

where p^* is the saturated vapor pressure of the pure component (Pa); A , B , C , and D are the evaporation constants for each element; and T is the absolute temperature (K). The relationship between the saturated vapor pressure and temperature of Mg, Ca, Mn, Al, Fe, Si, and Ti element is plotted in Figure 3a [17]. Clearly, the saturated vapor pressure of each pure element significantly increases with the increasing temperature, and the saturated vapor pressure of pure manganese is second only to Ca and Mg at 1600°C , reaching up to 5370 Pa, indicating that manganese is extremely volatilized into vapor phase under vacuum.

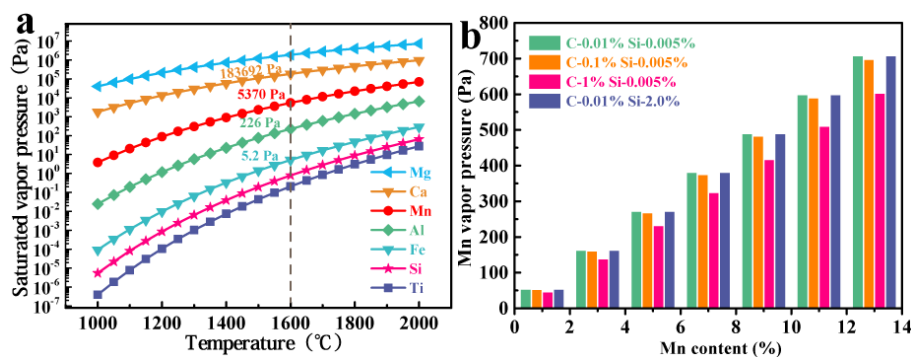


Figure 3. (a) Vapor pressure as a function of temperature for different pure metal elements. (b) The partial vapor pressure of manganese component in steel with different initial manganese content, which is affected by carbon and silicon content.

Furthermore, the partial vapor pressure (p_{Mn}) of different content manganese components (Table 3) in molten steel, based on the thermodynamic equilibrium between liquid and vapor phases, can be expressed by the following Equation (2) [18]:

$$p_{Mn} = x_{Mn} r_{Mn} p^* = \frac{56}{5500} f_{Mn} w_{Mn} p^* \quad (2)$$

where x_{Mn} is the molar fraction of manganese in the molten steel; r_{Mn} is the Raoultian activity coefficient of Mn; and f_{Mn} and w_{Mn} are the activity coefficient and mass percentage based on 1% concentration in Henry's Law. According to Wagner's model [19], the interaction coefficients (Table 4) at the same temperature (1873 K) are used to calculate the activity coefficients in Equation (3).

$$\lg f_{Mn} = e_{Mn}^C w_C + e_{Mn}^{Si} w_{Si} + e_{Mn}^{Mn} w_{Mn} + e_{Mn}^P w_P + e_{Mn}^S w_S + e_{Mn}^{Al} w_{Al} + e_{Mn}^{Ti} w_{Ti} + e_{Mn}^O w_O + e_{Mn}^N w_N \quad (3)$$

Table 3. Chemical composition of different Mn content in steel, wt%.

Composition	(C)	(Si)	(Mn)	(P)	(S)	(Al)	(Ti)	T. O	(N)
Mn-1%	0.01	0.005	2	0.017	0.009	0.036	0.056	0.002	0.003
Mn-3%	0.01	0.005	3	0.017	0.009	0.036	0.056	0.002	0.003
Mn-5%	0.01	0.005	5	0.017	0.009	0.036	0.056	0.002	0.003
Mn-7%	0.01	0.005	7	0.017	0.009	0.036	0.056	0.002	0.003
Mn-9%	0.01	0.005	9	0.017	0.009	0.036	0.056	0.002	0.003
Mn-11%	0.01	0.005	11	0.017	0.009	0.036	0.056	0.002	0.003
Mn-13%	0.01	0.005	13	0.017	0.009	0.036	0.056	0.002	0.003

Table 4. Interaction coefficient of elements at 1873 K.

Composition	(C)	(Si)	(Mn)	(P)	(S)	(Al)	(Ti)	T. O	(N)
Mn	-0.07	0	0	-0.0035	-0.048	0	0	-0.083	-0.091

The partial vapor pressure (p_{Mn}) of the manganese component is a function of manganese, carbon, and silicon contents, as shown in Figure 3b. It can be clearly seen that the partial vapor pressure of the manganese component increases with the increase of manganese content in molten steel, proving that the high manganese content can facilitate volatilization. In addition, the carbon content in the molten steel has evident effects on the partial vapor pressure of manganese in the same conditions of manganese and silicon content, and a higher carbon content in steel leads to a lower partial vapor pressure of manganese. When the content of silicon increases to 2.0%, the partial vapor pressure of manganese still remains, revealing the partial vapor pressure of manganese is not affected by the silicon content, which is attributed to the interaction coefficient of silicon to manganese that is equal to 0.

3.2. Effects of Alloying Methods on the Manganese Volatilization

To evaluate the effect different alloying methods on volatilization behavior of manganese in molten steel, the high-carbon ferromanganese and silicon manganese alloy were added during the vacuum process and investigated. The steel samples and ingots obtained are shown in Figure 4a. Figure 4b shows acicular ferrite structure in the ingot, and the corresponding EPMA mapping for manganese element, which indicates manganese element presented severe dendrite segregation, also proving that the existence forms of manganese in the steel.

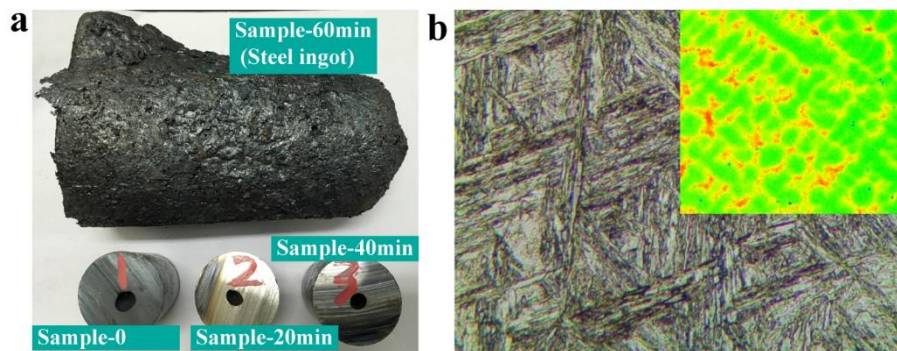


Figure 4. (a) The steel sample. (b) Micrograph of steel ingot and corresponding (inset of Figure 4b) EPMA element distribution of manganese element in steel ingot.

Furthermore, the analysis results of obtained steel samples are listed in Table 5. It is found that the content of manganese in molten steel with the addition of high-carbon ferromanganese and silicon manganese alloy present the same decreasing tendency with the extension of vacuum time. The content of manganese in molten steel with the alloying method of silicon manganese decreases rapidly in the first 20 min, from 11.05 to 8.95 wt%, which is attributed to the fast pressure drop result in the acceleration of the evaporation of manganese. The slow decrease of manganese content in molten steel in the latter stage and until 60 min reached 7.92 wt%, owing to the gradually decreasing partial vapor pressure caused by the reduced manganese content. Similarly, the content of manganese in molten steel with the addition of high-carbon ferromanganese had a slight attenuation from the initial 11.34 to 8.41 wt% for 60 min. It is confirmed that the increased carbon content in molten steel will lower the partial vapor pressure of component manganese, agreeing with the thermodynamic calculation results in Figure 3b. In addition, the carbon monoxide gas generated in the decarburization reaction of the molten steel in vacuum can also increase the pressure of the vacuum chamber, thus hindering the volatilization of manganese. Furthermore, the effect mechanism of silicon and carbon element on the volatilization of manganese requires more in-depth research.

Table 5. Measured chemical compositions of steel samples (wt%).

Alloying Methods	Holding Time (min)	(C)	(Mn)	(Al)	(Si)	(P)	(S)
High-carbon ferromanganese	0	0.838	11.337	0.016	0.064	0.039	0.005
	20	0.815	10.185	0.011	0.085	0.041	0.006
	40	0.797	9.184	0.063	0.097	0.040	0.006
	60	0.770	8.410	0.075	0.099	0.042	0.006
Silicon manganese	0	0.294	11.051	0.180	2.641	0.033	0.008
	20	0.272	8.950	0.189	2.671	0.036	0.008
	40	0.246	8.532	0.223	2.622	0.033	0.007
	60	0.238	7.921	0.229	2.620	0.034	0.007

3.3. Analysis of Manganese Volatile Phase

The morphologies of high-carbon ferromanganese and silicon manganese alloy conducted by field-emission scanning electron microscopy (FESEM) are shown in Figure 5, and irregular lump shape was observed. As for volatile fraction generated in the vacuum process, which was condensed on the inner wall of the vacuum chamber and deposit to a certain thickness, it can be observed in Figure 6a, b. To further explore the effects of different alloying methods on manganese volatile phase structure, XRD analysis of volatile fraction, in addition to high-carbon ferromanganese and silicon manganese, was carried out. As shown in Figure 6c, the volatile fraction generated in the alloying method of high-carbon ferromanganese was mainly composed of MnO (JCPDS No. 89-2804) and a small amount

of Mn_3O_4 (JCPDS No. 75-1560) and Mn (JCPDS No. 17-910). The appearance of manganese oxide phase is attributed to continuous evaporation of manganese at first condensation on the inner wall of the vacuum chamber and then oxidized by air, to form Mn_xO , after opening the furnace door. After the silicon manganese was added, the main phase of volatile fraction was transformed into Mn_3O_4 , and a small number of Mn and MnO phases were generated (Figure 6d). This may be correlated to the particle size of volatile manganese, which affects the thermodynamic stability of manganese oxide phase [20].

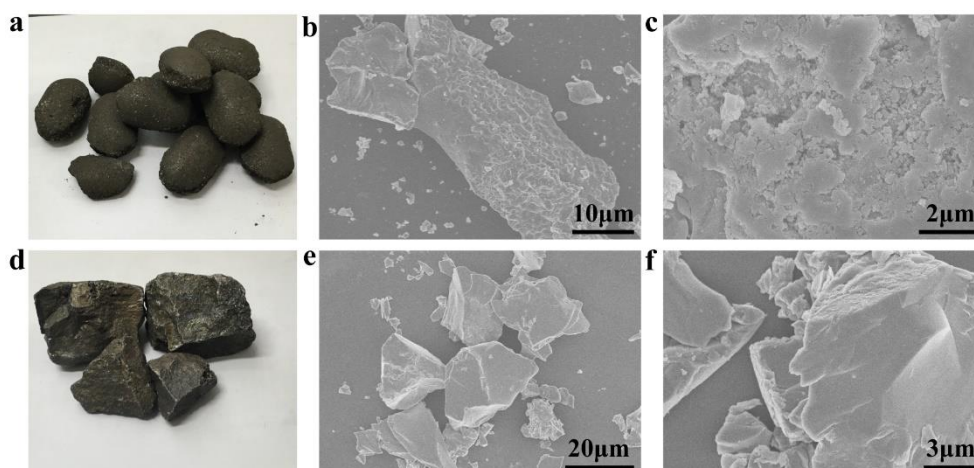


Figure 5. The physical drawing and FESEM image of (a–c) high-carbon ferromanganese and (d–f) silicon manganese.

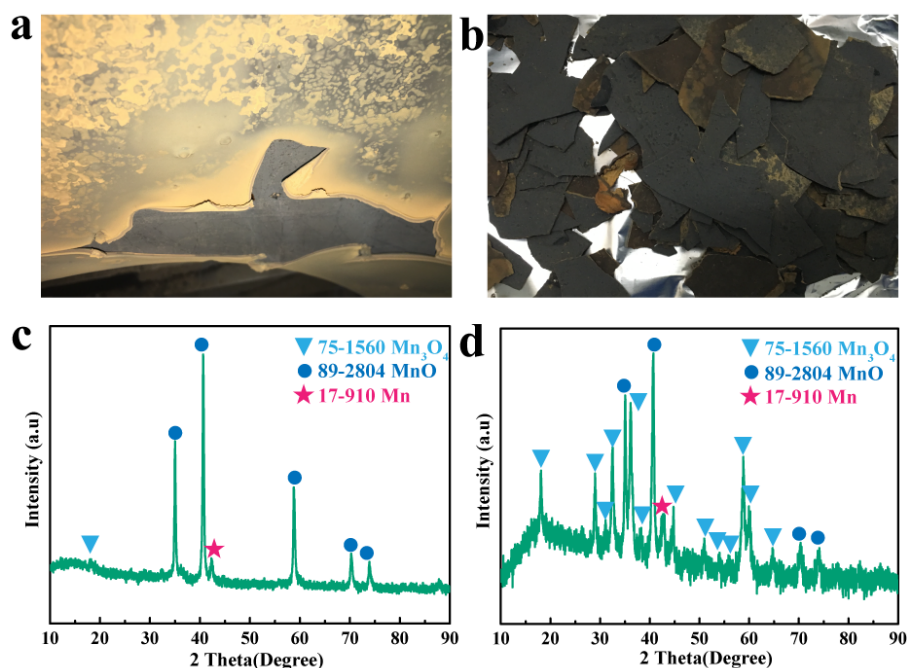


Figure 6. (a,b) The physical drawing of volatile fraction condensed inside the vacuum chamber after vacuum treatment. XRD patterns of volatile fraction with different alloying methods of (c) high-carbon ferromanganese and (d) silicon manganese.

Simultaneously, the morphology of volatile fraction was characterized by FESEM, which is completely different from the morphology of the manganese alloy, further confirming that the volatile fraction only comes from the volatilization of manganese element in the molten steel. As shown in the FESEM images in Figure 7a,b, volatile fraction generated in alloying method of high-carbon

ferromanganese exhibited a nanoscale morphology, including a large amount of nanorods with a lateral length approximately 500 nm and a small number of particles with less than 500 nm. Based on XRD analysis results, the nanorod structure can be ascribed to MnO phase. In contrast, all uneven nanoparticles with a diameter less than 500 nm can be discovered in Figure 7c,d, which corresponds to volatile fraction generated in alloying method of silicon manganese. It is worth mentioning that the volatile manganese was oxidized owing to the high chemical activity of nanoscale particles [21]. Besides this, the EDS mapping images (Figure 7e) further verify element Mn and O uniform distributed in entire nanoparticles, matching well with XRD analysis results. In addition, the corresponding element content analysis (inset of Figure 7e) shows that the mass fraction of Mn and O is 82.67% and 17.33%, respectively, confirming the existence of the manganese oxide phase.

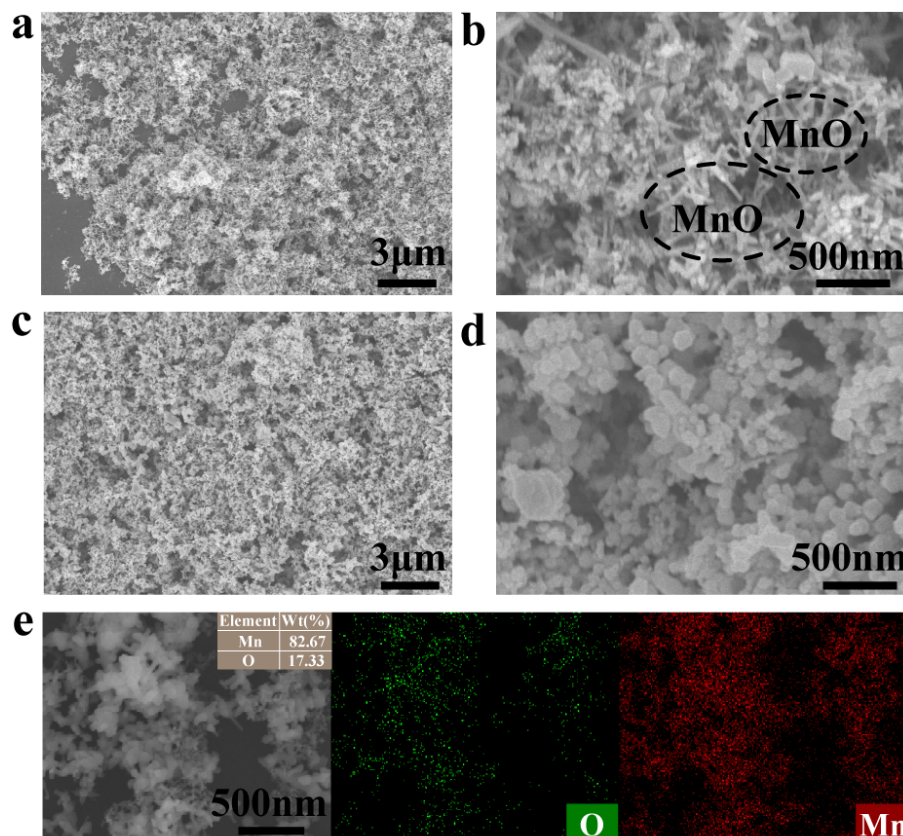


Figure 7. FESEM images of volatile fraction with different alloying methods of (a,b) high-carbon ferromanganese and (c,d) silicon manganese. (e) X-ray energy dispersive spectrometry (EDS) of volatile fraction with alloying methods of silicon manganese.

4. Conclusions

In the current study, thermodynamic calculation was performed to determine the partial vapor pressure of manganese component in molten steel. The volatilization behavior of manganese was investigated by laboratory experiments for manganese steels, with different alloying methods, in vacuum process. The following conclusions can be obtained:

1. With the increase of manganese content, the partial vapor pressure of manganese component increased, resulting in manganese components being easily volatilized from molten steel. Moreover, the greater the carbon content in the steel, the lower the partial vapor pressure of manganese component. However, the partial vapor pressure of manganese component is not influenced by the silicon content in molten steel, which is depends on the value of the interaction coefficient.

2. As a result, an obvious decrease trend of manganese content in the steel under vacuum process with time can be found. Compared with the alloying method of high-carbon ferromanganese, the volatilization loss of manganese in the alloying method of silicon manganese presents faster decay. The observed results were in good agreement with thermodynamic analysis.
3. The volatile fraction generated in alloying method of high-carbon ferromanganese is composed of a large amount of MnO nanorods with a lateral length approximately 500 nm and a small number of Mn₃O₄/Mn nanoparticles with diameter less than 500 nm. Meanwhile, the volatile fraction generated in alloying method of silicon manganese shows Mn₃O₄ nanoparticles as the main phase. It can be inferred that the existence of the manganese oxide phase is attributed to the high chemical activity of nanoscale particles in air.

Author Contributions: Investigation, J.C. and Y.B.; project administration, J.C.; writing—original draft, J.C.; writing—review and editing, J.C. and Y.B.; and funding acquisition, Y.B. All authors have read and agreed to the published version of the manuscript.

Funding: This work was supported by the National Natural Science Foundation of China (Grant No. 51874021).

Conflicts of Interest: The authors declare no competing interest.

References

1. Jacob, R.; Raman Sankaranarayanan, S.; Kumares Babu, S.P. Recent advancements in manganese steels—A review. *Mater Today Proc.* **2020**, *27*, 2852–2858. [[CrossRef](#)]
2. Chen, J.; Ren, J.-K.; Liu, Z.-Y.; Wang, G.-D. The essential role of niobium in high manganese austenitic steel for application in liquefied natural gas tanks. *Mater. Sci. Eng. A* **2020**, *772*, 138733. [[CrossRef](#)]
3. Lv, C.; Wang, Y.; Huang, X.; Zhang, L.; Fu, Q.; Wu, M.; Zhang, J.; Wang, Y.H.; Fu, Q.Q.; Min, W.; et al. The novel combination of strength and ductility in 0.4C-7Mn-3.2Al medium manganese steel by intercritical annealing. *Steel Res. Int.* **2019**, *90*. [[CrossRef](#)]
4. Li, Y.; Li, W.; Min, N.; Liu, W.; Zhang, C.; Jin, X. Mechanical response of a medium manganese steel with encapsulated austenite. *Scr. Mater.* **2020**, *178*, 211–217. [[CrossRef](#)]
5. Cao, R.; Liang, J.; Li, F.; Li, C.; Zhao, Z. Intercritical annealing processing and a new type of quenching and partitioning processing, actualized by combining intercritical quenching and tempering, for medium manganese lightweight steel. *Steel Res. Int.* **2019**, *91*. [[CrossRef](#)]
6. Ezatpour, H.; Torabi-Parizi, M.; Ebrahimi, G.R.; Momeni, A. Effect of micro-alloy elements on dynamic recrystallization behavior of a high-manganese steel. *Steel Res. Int.* **2018**, *89*. [[CrossRef](#)]
7. Wang, M.; Jiang, M.; Tazan, C.C. Manganese micro-segregation governed austenite re-reversion and its mechanical effects. *Scr. Mater.* **2020**, *179*, 75–79. [[CrossRef](#)]
8. Cao, Y.; Luo, C.; Zhao, L.; Peng, Y.; Song, L.; Ma, C.-Y.; Tian, Z.-L.; Zhong, M.-L.; Wang, Y.-J. Microstructural evolution and mechanical properties of laser-welded joints of medium manganese steel. *J. Iron Steel Res. Int.* **2019**, *27*, 75–87. [[CrossRef](#)]
9. Peixoto, J.J.M.; Gabriel, W.V.; De Oliveira, T.A.S.; Da Silva, C.A.; Da Silva, I.A.; Seshadri, V. Numerical simulation of recirculating flow and physical model of slag–metal behavior in an RH reactor: Application to desulfurization. *Met. Mater. Trans. A* **2018**, *49*, 2421–2434. [[CrossRef](#)]
10. Zhang, L.-F.; Li, F. Investigation on the fluid flow and mixing phenomena in a Ruhrstahl-Heraeus (RH) steel degasser using physical modeling. *JOM* **2014**, *66*, 1227–1240. [[CrossRef](#)]
11. Van Ende, M.-A.; Kim, Y.-M.; Cho, M.-K.; Choi, J.; Jung, I.-H. A kinetic model for the Ruhrstahl Heraeus (RH) degassing process. *Met. Mater. Trans. A* **2011**, *42*, 477–489. [[CrossRef](#)]
12. Deng, Z.; Kong, L.; Liang, N.; Zhu, M. Reaction of Al-killed manganese steel with ladle slag. *Steel Res. Int.* **2019**, *90*. [[CrossRef](#)]
13. Kong, L.; Deng, Z.; Cheng, L.; Zhu, M. Reaction behaviors of Al-killed medium-manganese steel with glazed MgO refractory. *Met. Mater. Trans. A* **2018**, *49*, 3522–3533. [[CrossRef](#)]
14. Huang, A.; Wang, Y.; Zou, Y.; Gu, H.; Fu, L. Dynamic interaction of refractory and molten steel: Corrosion mechanism of alumina-magnesia castables. *Ceram. Int.* **2018**, *44*, 14617–14624. [[CrossRef](#)]

15. Van Ende, M.-A.; Guo, M.; Dekkers, R.; Burty, M.; Van Dyck, J.; Jones, P.T.; Blanpain, B.; Wollants, P. Formation and evolution of Al–Ti oxide inclusions during secondary steel refining. *ISIJ Int.* **2009**, *49*, 1133–1140. [[CrossRef](#)]
16. Zhang, Z.; Wang, Z.; Chen, D.; Miao, R.; Zhu, Q.; Zhang, X.; Zhou, L.; Li, Z.-A. Purification of praseodymium to 4N5+ purity. *Vacuum* **2014**, *102*, 67–71. [[CrossRef](#)]
17. Dai, Y.N.; Yang, B. *Vacuum Metallurgy of Nonferrous Metal Materials*, 1st ed.; Metallurgical Industry Press: Beijing, China, 2000.
18. Reimer, C.; Jourdan, J.; Bellot, J.-P. Ti-17 volatilization under vacuum: Investigation of the activity coefficients at 1900 °C. *Calphad* **2017**, *58*, 122–127. [[CrossRef](#)]
19. Guo, H.J. *Metallurgical Physical Chemistry Course*, 2nd ed.; Metallurgical Industry Press: Beijing, China, 2006.
20. Birkner, N.; Navrotsky, A. Thermodynamics of manganese oxides: Effects of particle size and hydration on oxidation-reduction equilibria among hausmannite, bixbyite, and pyrolusite. *Am. Miner.* **2012**, *97*, 1291–1298. [[CrossRef](#)]
21. Navrotsky, A. Nanoscale effects on thermodynamics and phase equilibria in oxide systems. *ChemPhysChem* **2011**, *12*, 2207–2215. [[CrossRef](#)] [[PubMed](#)]



© 2020 by the authors. Licensee MDPI, Basel, Switzerland. This article is an open access article distributed under the terms and conditions of the Creative Commons Attribution (CC BY) license (<http://creativecommons.org/licenses/by/4.0/>).